Nanoscale

COMMUNICATION

View Article Online
View Journal | View Issue

Cite this: *Nanoscale*, 2015, **7**, 4900

Received 30th November 2014,
Accepted 2nd February 2015

DOI: 10.1039/c4nr07074g

www.rsc.org/nanoscale

NiO_x-Fe_2O_3-coated p-Si photocathodes for enhanced solar water splitting in neutral pH water†

Alireza Kargar,[a] Justin S. Cheung,[a] Chin-Hung Liu,[b,c] Tae Kyoung Kim,[b,c] Conor T. Riley,[d] Shaohua Shen,[e] Zhaowei Liu,[a] Donald J. Sirbuly,[d] Deli Wang[a,b,f] and Sungho Jin*[b,c]

We report successful growth of a uniform and scalable nanocomposite film of Fe_2O_3 nanorods (NRs) and NiO_x nanoparticles (NPs), their properties and application for enhanced solar water reduction in *neutral* pH *water* on the surface of p-Si photocathodes.

Photoelectrochemical (PEC) hydrogen production through solar water splitting is one of the promising clean routes to renewable energy sources to minimize the dependence on polluting energy sources,[1–9] and can lead to high solar-to-hydrogen (STH) efficiencies of up to 31.1%.[10] To obtain such high efficiencies for long-time PEC operation, however, major challenges remain in design and engineering of cost-effective stable photoelectrodes which can offer bias-free photoactivity for efficient full PEC systems/devices. Furthermore, obtaining such a performance in neutral pH water is highly desirable as the natural water resources such as seawater are usually in a neutral condition, and are abundant and easily disposable. Employing a neutral electrolyte for solar water splitting also prevents the undesirable use of strong acids or bases, which can lead to environmental and handling issues.

Silicon is one of the promising materials for the PEC cells considering its unique properties as well as mature fabrication industry.[8,11–23] However from the electrochemical point of view, the surface of Si photoelectrodes has poor catalytic activity (kinetic limitation) for the hydrogen evolution reaction (HER) or oxygen evolution reaction (OER). To accelerate the HER or OER for achieving sufficient hydrogen production, it is essential that a catalyst is added to the electrode surface. Metal oxides have shown promising potential to catalyze the Si surface,[15,24–26] in which they can also simultaneously stabilize the Si surface against corrosion/oxidation.[15,24,26] We have demonstrated that ZnO nanowires (NWs)[12,27] can catalyze the surface of p-Si NWs for the enhanced HER revealing promise to investigate other suitable metal oxides for more efficient HER on the surface of p-Si photocathodes. NiO, a wide band gap metal oxide, can be used as an OER catalyst,[25,28–30] or a HER catalyst/cocatalyst.[29,31–36]

In this article, we report facile solution growth of novel nanocomposite films consisting of Fe_2O_3 nanorods (NRs) and NiO_x nanoparticles (NPs), which are used to improve the HER on the inactive surface of p-Si film photocathodes in neutral pH water. Very interestingly, the new NiO_x-Fe_2O_3-coated p-Si photocathodes show photoactivity at 0 V *versus* the reversible hydrogen electrode (RHE) with a cathodic onset potential of 0.25 V *versus* RHE in neutral pH water. The achieved performance at zero bias in neutral solution shows promising application of the newly developed photoelectrodes.

Boron doped (p-type) Si(100) wafers with a resistivity of 1–20 Ω cm were cleaned with a buffered oxide etching (BOE) solution for 10 s, rinsed with deionized (DI) water, and dried with N_2 flow. Then, they were immediately transferred to the sputtering machine to deposit a thin SnO_2 layer as a seeding layer for the α-Fe_2O_3 NR film growth using RF magnetron sputtering with 99.99% SnO_2 target and argon gas at room temperature. The sputtering pressure was ~10 mTorr during the deposition. The α-Fe_2O_3 NR film was finally grown on the substrate using a hydrothermal growth method reported elsewhere with slight modification.[37] Akaganeite (β-FeOOH) NRs were first grown on the SnO_2-coated Si substrate by immersing them in a 45 mL sealed Teflon autoclave containing a 30 mL aqueous solution consisting of 0.15 M $FeCl_3 \cdot 6H_2O$ (iron(III) chloride hexahydrate) (Sigma-Aldrich, ≥99%) and 1 M $NaNO_3$

[a]*Department of Electrical and Computer Engineering, University of California-San Diego, La Jolla, California 92093, USA*
[b]*Materials Science and Engineering Program, University of California-San Diego, La Jolla, California 92093, USA. E-mail: jin@ucsd.edu; Fax: +1 858 5345698; Tel: +1 858 5344903*
[c]*Department of Mechanical and Aerospace Engineering, University of California-San Diego, La Jolla, California 92093, USA*
[d]*Department of Nanoengineering, University of California-San Diego, La Jolla, California 92093, USA*
[e]*State Key Laboratory of Multiphase Flow in Power Engineering, Xi'an Jiaotong University, Xi'an, Shaanxi 710049, China*
[f]*Qualcomm Institute (QI), University of California-San Diego, La Jolla, California 92093, USA*
†Electronic supplementary information (ESI) available. See DOI: 10.1039/c4nr07074g

(sodium nitrate) (Sigma-Aldrich, ≥99.0%). The DI water resistivity and pH of the growth solution were 17.6–17.7 MΩ cm and ~1.44, respectively. The hydrothermal reaction was performed at a temperature of ~110 °C, placing the autoclave in a regular oven for 2 h. The as-prepared sample was then rinsed carefully with DI water to remove the residues and dried with N_2 flow. After the FeOOH NR growth, the color of the Si substrate turned yellowish indicating the FeOOH growth. Finally, the as-grown FeOOH-SnO_2-coated Si substrate was annealed at 450 °C in air for 2 h to have a phase transition from β-FeOOH to α-Fe_2O_3, which was evident with the yellowish color changing to a reddish color. For convenience, Fe_2O_3 NRs synthesized from 2 h FeOOH NRs with subsequent 2 h annealing in air are denoted as 2 h-Fe_2O_3 NRs. The NiO_x solution was prepared with 0.12 M monoethanolamine (MEA, C_2H_7NO) (Sigma-Aldrich) and 0.05 M nickel acetate tetrahydrate ($Ni(OCOCH_3)_2{\cdot}4H_2O$) (Sigma-Aldrich) in 10 mL ethanol. Then, the as-prepared solution was spin-coated on the p-Si or Fe_2O_3-SnO_2-coated p-Si substrates with subsequent annealing at 300 °C for 30 s on a hot plate. Fig. 1 shows the fabrication procedure for the metal–oxide-coated p-Si substrates. For Pt catalyst deposition, electron beam (e-beam) evaporation was used to deposit 2 nm Pt at a base pressure of 6×10^{-7} Torr and a deposition rate of 0.2 Å s^{-1} on the SnO_2-coated p-Si substrates. To minimize the incident light loss, such a thin thickness for Pt was selected to provide a non-continuous film in the form of nanoparticles.

The sample morphology was examined using a Philips XL30 field-emission environmental scanning electron microscope (ESEM) working at an accelerating voltage of 10.0 kV. X-ray photoelectron spectra (XPS) were obtained using a Kratos spectrometer (AXIS Ultra DLD) with monochromatic Al K_α radiation ($h\nu$ = 1486.69 eV) and a concentric hemispherical analyzer. Optical absorption measurements were obtained using a 150 mm integrating sphere connected to a LAMBDA 1050 UV/Vis/NIR spectrophotometer.

To evaluate the sample performances, they were bonded to Cu wire at the back using indium, which provides an ohmic contact to the used p-type Si substrate. The edges and backside of samples were sealed using epoxy (Hysol 1C). Current density measurements were performed in a 200 mL aqueous solution of 0.25 M Na_2SO_4 buffered at pH = 7.1 with Phosphate Buffered Saline (PBS, Sigma) (DI water resistivity, 18.2 MΩ cm) (neutral pH water) with a three-electrode setup, including the sample as the working electrode (WE), Pt foil as the counter electrode (CE), and Ag/AgCl (1 M KCl) as the reference electrode (RE). A light power intensity of 100 mW cm^{-2} was tuned at the sample position using a solar simulator (Newport 66905) with a xenon lamp equipped with a 1.5 AM filter. The current density measurements were performed using a potentiostat (Digi-Ivy, DY2300). A scan rate of 10 mV s^{-1} was employed for the linear sweep voltammetry (LSV) and cyclic voltammetry (CV) measurements, unless otherwise stated. During the current density measurements, mild agitation was used and the electrolyte was constantly purged with a small flow of N_2 gas. The applied potentials *versus* Ag/AgCl RE ($E_{Ag/AgCl}$) were converted to the potentials *versus* the reversible hydrogen electrode (RHE), E_{RHE}, using the Nernst equation as follows:

$$E_{RHE} = E_{Ag/AgCl} + 0.059\ pH + E^0_{Ag/AgCl}\ (V) \quad (1)$$

where pH is the electrolyte pH (7.1 here) and $E^0_{Ag/AgCl}$ = 0.222 V for the Ag/AgCl RE in 1 M KCl and at 25 °C (Digi-Ivy, Inc.).

Fig. 2 shows scanning electron microscopy (SEM) images of 2 h-Fe_2O_3 NRs, which form a nearly continuous but individually separated NR film, grown on the p-Si substrate coated with a SnO_2 seeding layer (this structure is referred to as "Fe_2O_3-SnO_2-coated p-Si" hereafter). The thickness values of the Fe_2O_3 NR film and the SnO_2 seeding layer are ~141 nm and ~82 nm, respectively. The NRs form a vertically elongated textured film (Fig. 2b and 2c), increasing the optical absorption and electrochemical reaction surface area. The Fe_2O_3 NR growth is uniform over the large area (Fig. 2d) indicating the potential of scaling up the fabricated electrodes. Due to the small size of NiO_x NPs, we were not able to observe them under the SEM.

The X-ray diffraction (XRD) analysis of 2 h-Fe_2O_3 NRs grown on the fluorine-doped tin oxide (FTO) substrate (data not

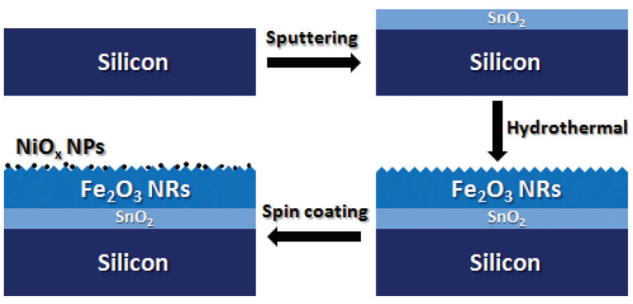

Fig. 1 Schematic representation of the fabrication procedure for the metal–oxide-coated p-Si substrates.

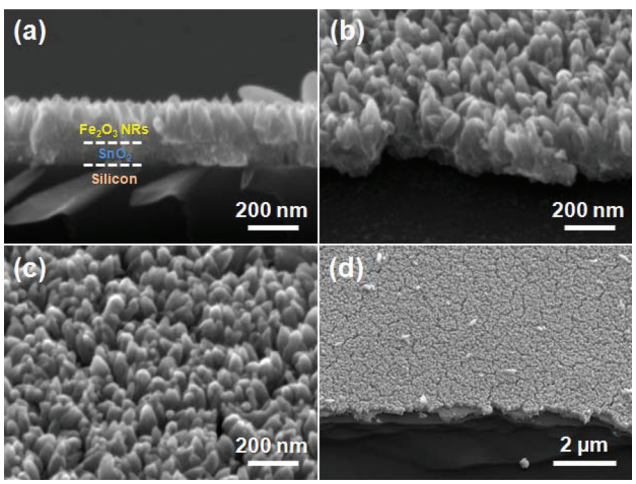

Fig. 2 High-magnification (a) cross-sectional and (b) tilted view SEM images of 2 h-Fe_2O_3 NRs grown on the p-Si substrate using SnO_2 as a seeding layer. (c) High- and (d) low-magnification 45° view SEM images of the corresponding sample.

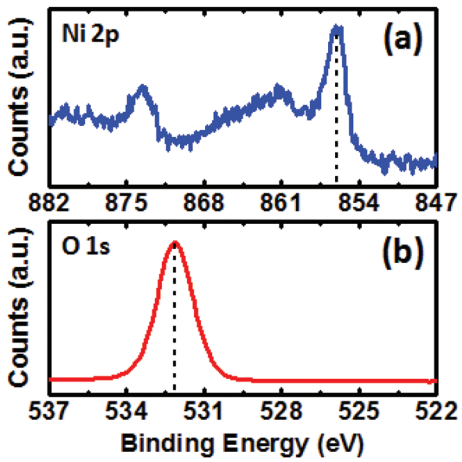

Fig. 3 (a) Ni 2p and (b) O 1s XPS spectra of NiO_x NPs spin-coated on the Si substrate.

shown here) exhibited the characteristic peaks of α-Fe_2O_3 (hematite). The XPS spectra of Ni 2p and O 1s of NiO_x NPs spin-coated on the Si substrate are shown in Fig. 3a and 3b revealing the chemical composition of NiO_x. The nickel XPS spectrum (Fig. 3a) shows four peaks including a dominant 2p3/2 peak at a binding energy of 856.2 eV, a 2p1/2 peak at 873.5 eV (these two are Ni peaks), and two small satellite peaks at 861.2 eV and 880.6 eV. The satellite peaks are because of the X-ray source emitting X-rays of higher photon energy leading to nickel ionization. The oxygen XPS spectrum (Fig. 3b) exhibits only an O 1s peak corresponding to a binding energy of 532.1 eV. Therefore, there is good NiO_x formation with the dominant Ni 2p3/2 peak at 856.2 eV and the O 1s peak at 532.1 eV.

The PEC performance of p-Si substrates with different metal oxide coatings is shown in Fig. 4, in which all the samples exhibit photocathodic behavior in the scanned potential range. The Fe_2O_3-SnO_2-coated p-Si sample provides a much higher photocurrent than the bare or SnO_2-coated p-Si substrates due to enhanced optical absorption originating from the textured surface and coupling of materials with different band gaps (see ESI and Fig. S1†), improved charge separation coming from the junctions between p-Si, n-SnO_2 and n-Fe_2O_3 (see ESI and Fig. S2†), and the increased reaction surface area coming from the NRs as shown in SEM images. As the optical absorption of the Fe_2O_3-SnO_2-coated p-Si sample significantly increases compared to the bare p-Si substrate, we believe that the absorption enhancement and after that improved charge separation play key roles in the performance enhancement. Due to coupling of Si and Fe_2O_3 with ~1.11 eV and ~2.1 eV band gaps, respectively, the Fe_2O_3-SnO_2-coated p-Si substrate can provide a broadband spectral photoresponse and incident photon-to-current efficiency (IPCE).[38] The NiO_x NP coating also improves the photocurrent of the p-Si substrate which can be because of the catalytic effect of NiO_x NPs. The NiO_x NPs do not change the optical absorption of the p-Si substrate in a significant way (see Fig. S1†) probably due to the

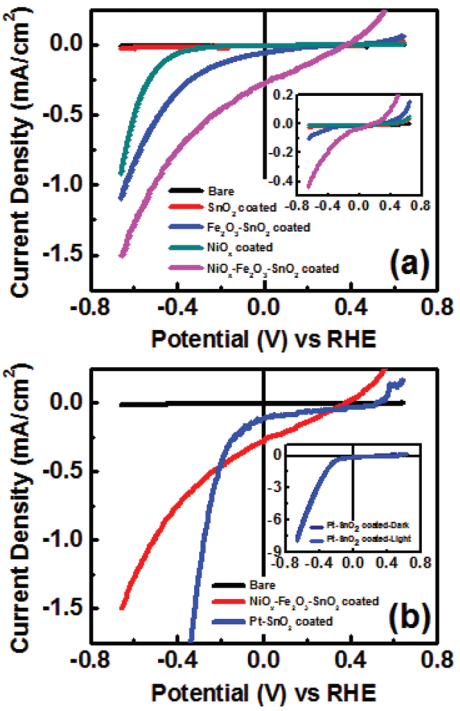

Fig. 4 Current density under illumination of different metal–oxide-coated p-Si photocathodes measured in neutral pH water. The inset shows the dark current of the corresponding samples. (b) Current density under illumination of bare and NiO_x-Fe_2O_3-SnO_2-coated p-Si photocathodes in comparison with the Pt-SnO_2-coated p-Si photocathode measured in neutral pH water. The inset shows the current density of the Pt-SnO_2-coated p-Si photocathode in the dark and under illumination. The scan rate was 10 mV s^{-1}.

very thin and discontinuous NiO_x coating layer in the form of very small NPs and a NiO_x large band gap. Note that the Fe_2O_3-SnO_2 coating layer is more effective in enhancing the photocathodic performance than the NiO_x NP coating layer especially for photoactivity at 0 V *versus* RHE (as shown in Fig. 4a) due to the aforementioned Fe_2O_3-SnO_2 layer properties. Using NiO_x NPs on the Fe_2O_3-SnO_2-coated p-Si substrate (this structure is called "NiO_x-Fe_2O_3-SnO_2-coated p-Si" hereafter), the photocurrent significantly increases resulting in a net photocathodic current (light current–dark current) of 0.25 mA cm^{-2} at 0 V *versus* RHE and a cathodic onset potential of 0.25 V *versus* RHE. Note that the onset potential is calculated when the photocurrent reaches a value of −0.1 mA cm^{-2}. The onset potential shift of the NiO_x-Fe_2O_3-SnO_2-coated p-Si photocathode is 0.7 V and 0.38 V compared to the onset potential of NiO_x-coated (which is −0.45 V *versus* RHE) and Fe_2O_3-SnO_2-coated (that is −0.13 V *versus* RHE) p-Si photocathodes, respectively. The photocurrent at zero bias and onset potential can be further improved (shifting the onset potential towards more positive potentials) using nanotextured Si substrates. These obtained results are really promising paving the way to achieve the overall spontaneous solar water splitting in a full PEC system/device working in neutral pH water.

The photocathodic performance of the NiO_x-Fe_2O_3-SnO_2-coated p-Si substrate is compared with that of the Pt-SnO_2-

coated p-Si photocathode (Fig. 4b) to see the effect of the NiO_x-Fe_2O_3 NR film compared to Pt NPs for the improved HER performance. The Pt-SnO_2-coated p-Si photocathode provides a lower current around 0 V *versus* RHE than the NiO_x-Fe_2O_3-SnO_2-coated p-Si photocathode with an onset potential of about 0 V *versus* RHE in the tested neutral solution. However, the Pt-SnO_2-coated p-Si photocathode offers a much higher current than the NiO_x-Fe_2O_3-SnO_2-coated p-Si substrate at higher reversed biasing potentials (see Fig. S3†). The achieved cathodic onset potential for the Pt-SnO_2-coated p-Si substrate is consistent with that reported for a nominally ~1 nm thick Pt coating using e-beam evaporation on the p-Si substrate in an electrolyte with a pH of 4.5[39] and the 5 nm thick Pt coating using e-beam evaporation on the sputtered-ZnO-coated p-Si substrate in a solution with a pH of 7.2.[40] In fact, the Pt-SnO_2-coated p-Si substrate does not provide significant photoactivity in which its current density in the dark and under illumination is almost the same (Fig. 4b inset). Note that the sputtered thin SnO_2 coating does not significantly improve the photocurrent of p-Si (see Fig. 4a). Direct Pt coating on the p-Si substrate also showed the same behavior of not having significant photoactivity, which is consistent with that reported before.[40] This is because e-beam evaporated Pt coating provides ohmic contact to the p-Si substrate leading to high catalytic activity but without enabling a photovoltage at the interface.[39] The type of Pt deposition technique affects the HER performance in which electroless deposition for Pt coating on the p-Si substrate can provide high photocurrent at 0 V *versus* RHE and a positive cathodic onset potential due to the fact that the electroless deposition provides an interfacial oxide barrier enabling a photovoltage at the interface.[11,39] A buried n^+p junction can be used to obtain a photovoltage leading to a high photocurrent at 0 V *versus* RHE and a positive onset potential for the e-beam-evaporated Pt coating on p-Si photocathodes.[11] Furthermore, the type of electrolyte significantly affects the performance of Pt-coated p-Si photocathodes in which acidic electrolytes provide much better performance than neutral solutions mainly due to the higher activity of Pt in acidic electrolytes.

The stability performance of the Fe_2O_3-SnO_2- and Pt-SnO_2-coated p-Si photocathodes is shown in Fig. 5. The Fe_2O_3-SnO_2 coating layer can stabilize the inherently unstable p-Si substrate. The orientation and morphology of the p-Si substrate can affect the stability performance of Fe_2O_3-SnO_2-coated p-Si photocathodes in which p-Si nanowires made with Si(111) wafer provide much longer stability without any significant morphological changes after long-term stability and with preservation of all materials.[38] There is a gradual performance degradation for the Pt-SnO_2-coated p-Si electrode in which its current density decreases over time which can be possibly due to detachment of Pt NPs from the substrate. Note that the SnO_2-coated p-Si photocathode is not stable and its photo-

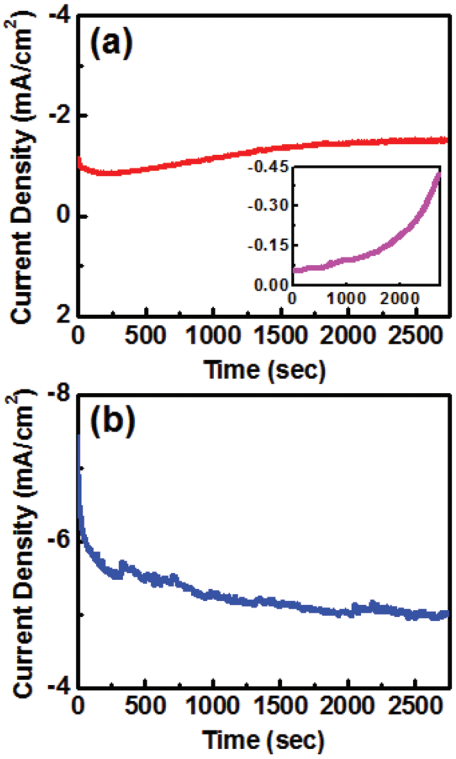

Fig. 5 Current density under illumination *versus* time (stability test) measured in neutral pH water at −0.66 V *versus* RHE of (a) the Fe_2O_3-SnO_2-coated p-Si photocathode and (b) the Pt-SnO_2-coated p-Si photocathode. The inset in (a) shows the stability test for the SnO_2-coated p-Si photocathode at −0.86 V *versus* RHE.

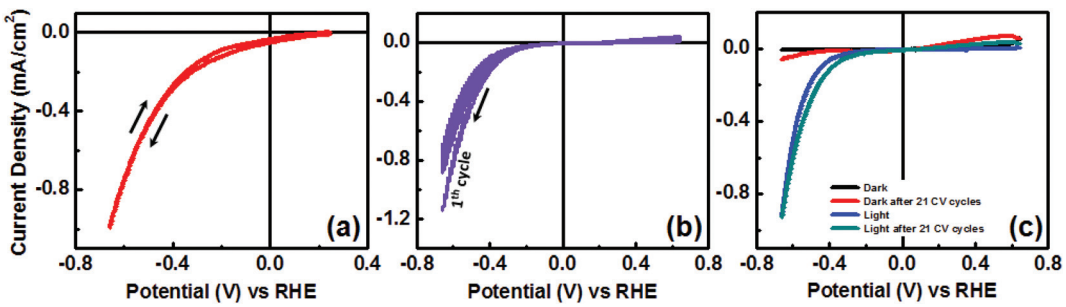

Fig. 6 Cyclic voltammetry (CV) under illumination of (a) Fe_2O_3-SnO_2-coated p-Si photocathode and (b) NiO_x-coated p-Si photocathode for 21 cycles measured in neutral pH water. (c) Current density under illumination and in the dark before and after 21 CV cycles for the NiO_x-coated p-Si photocathode tested in neutral pH water. The scan rate for (b) was 50 mV s^{-1}, and for (a) and (c) was 10 mV s^{-1}.

current continuously increases possibly due to SnO_2 dissolution in the electrolyte (Fig. 5a inset).

To further evaluate the stability performance of metal–oxide-coated p-Si substrates, we performed CV measurements as shown in Fig. 6. The Fe_2O_3-SnO_2-coated p-Si photocathode does not show any corrosive peak indicating preservation of all materials within this heterostructure, which was also investigated by SEM imaging after the PEC tests. The NiO_x-coated p-Si electrode was investigated in subsequent CV measurements (Fig. 6b) in which its photocurrent decreases a little and then reaches a stationary current level. There is no corrosive peak in all CV scans as can be seen from Fig. 6b. Although we did not observe any significant peak in the CV measurements indicating NiO_x transformation in the performed neutral electrolyte, the NiO_x NPs may be converted to $Ni(OH)_2$ or Ni NPs under the HER conditions.[32,33] The current density (LSV measurement) of the NiO_x-coated p-Si photocathode does not change significantly after the long CV measurement shown in Fig. 6b, indicating that a stable state is reached for the NiO_x catalyst on the p-Si substrate during the tested period. The NiO_x-Fe_2O_3-SnO_2-coated p-Si electrode also did not show any corrosive peak.

Conclusions

In summary, we showed facile and scalable solution growth of uniform NiO_x-Fe_2O_3 NR films, consisting of vertically aligned Fe_2O_3 NRs and coated NiO_x NPs. This new structure exhibited an improved solar water reduction characteristic in a neutral solution on the surface of p-Si film photocathodes leading to photoactivity at 0 V *versus* RHE and a cathodic onset potential of 0.25 V *versus* RHE. This study reveals the promising potential to design and engineer cost-effective Si/metal–oxide photoelectrodes for efficient solar water splitting under neutral and zero-bias conditions.

Acknowledgements

This work was supported by the Department of Energy (DOE DE-FG36-08G018016), the National Science Foundation (NSF ECCS0901113 and CBET1236155), and the Iwama Endowed Fund at UCSD. The authors thank Drs Ramesh Rao and Bernd Fruhberger of QI for their support. A.K. also acknowledges UCSD NANO3 staff especially Sean Park and Ivan Harris for their support and assistants.

Notes and references

1 J. R. McKone, N. S. Lewis and H. B. Gray, *Chem. Mater.*, 2013, **26**, 407–414.
2 G. Wang, Y. Ling and Y. Li, *Nanoscale*, 2012, **4**, 6682–6691.
3 M. S. Faber and S. Jin, *Energy Environ. Sci.*, 2014, **7**, 3519–3542.
4 B. A. Pinaud, J. D. Benck, L. C. Seitz, A. J. Forman, Z. Chen, T. G. Deutsch, B. D. James, K. N. Baum, G. N. Baum, S. Ardo, H. Wang, E. Miller and T. F. Jaramillo, *Energy Environ. Sci.*, 2013, **6**, 1983–2002.
5 M. G. Walter, E. L. Warren, J. R. McKone, S. W. Boettcher, Q. Mi, E. A. Santori and N. S. Lewis, *Chem. Rev.*, 2010, **110**, 6446–6473.
6 J. Kibsgaard, Z. Chen, B. N. Reinecke and T. F. Jaramillo, *Nat. Mater.*, 2012, **11**, 963–969.
7 Z. Lu, H. Wang, D. Kong, K. Yan, P.-C. Hsu, G. Zheng, H. Yao, Z. Liang, X. Sun and Y. Cui, *Nat. Commun.*, 2014, **5**, 5345.
8 S. Y. Reece, J. A. Hamel, K. Sung, T. D. Jarvi, A. J. Esswein, J. J. H. Pijpers and D. G. Nocera, *Science*, 2011, **334**, 645–648.
9 C. Liu, N. P. Dasgupta and P. Yang, *Chem. Mater.*, 2013, **26**, 415–422.
10 S. Hu, C. Xiang, S. Haussener, A. D. Berger and N. S. Lewis, *Energy Environ. Sci.*, 2013, **6**, 2984–2993.
11 S. W. Boettcher, E. L. Warren, M. C. Putnam, E. A. Santori, D. Turner-Evans, M. D. Kelzenberg, M. G. Walter, J. R. McKone, B. S. Brunschwig, H. A. Atwater and N. S. Lewis, *J. Am. Chem. Soc.*, 2011, **133**, 1216–1219.
12 K. Sun, Y. Jing, C. Li, X. Zhang, R. Aguinaldo, A. Kargar, K. Madsen, K. Banu, Y. Zhou, Y. Bando, Z. Liu and D. Wang, *Nanoscale*, 2012, **4**, 1515–1521.
13 M. T. Mayer, C. Du and D. Wang, *J. Am. Chem. Soc.*, 2012, **134**, 12406–12409.
14 S. Hu, M. R. Shaner, J. A. Beardslee, M. Lichterman, B. S. Brunschwig and N. S. Lewis, *Science*, 2014, **344**, 1005–1009.
15 J. Yang, K. Walczak, E. Anzenberg, F. M. Toma, G. Yuan, J. Beeman, A. Schwartzberg, Y. Lin, M. Hettick, A. Javey, J. W. Ager, J. Yano, H. Frei and I. D. Sharp, *J. Am. Chem. Soc.*, 2014, **136**, 6191–6194.
16 M. J. Kenney, M. Gong, Y. Li, J. Z. Wu, J. Feng, M. Lanza and H. Dai, *Science*, 2013, **342**, 836–840.
17 J. Oh, T. G. Deutsch, H.-C. Yuan and H. M. Branz, *Energy Environ. Sci.*, 2011, **4**, 1690–1694.
18 S. K. Cho, F.-R. F. Fan and A. J. Bard, *Angew. Chem., Int. Ed.*, 2012, **51**, 12740–12744.
19 S. W. Boettcher, J. M. Spurgeon, M. C. Putnam, E. L. Warren, D. B. Turner-Evans, M. D. Kelzenberg, J. R. Maiolo, H. A. Atwater and N. S. Lewis, *Science*, 2010, **327**, 185–187.
20 Y. W. Chen, J. D. Prange, S. Dühnen, Y. Park, M. Gunji, C. E. D. Chidsey and P. C. McIntyre, *Nat. Mater.*, 2011, **10**, 539–544.
21 C. Liu, J. Tang, H. M. Chen, B. Liu and P. Yang, *Nano Lett.*, 2013, **13**, 2989–2992.
22 A. Kargar, K. Sun, Y. Jing, C. Choi, H. Jeong, Y. Zhou, K. Madsen, P. Naughton, S. Jin, G. Y. Jung and D. Wang, *Nano Lett.*, 2013, **13**, 3017–3022.
23 J. Shi, Y. Hara, C. Sun, M. A. Anderson and X. Wang, *Nano Lett.*, 2011, **11**, 3413–3419.
24 K. Jun, Y. S. Lee, T. Buonassisi and J. M. Jacobson, *Angew. Chem., Int. Ed.*, 2012, **51**, 423–427.

25 K. Sun, N. Park, Z. Sun, J. Zhou, J. Wang, X. Pang, S. Shen, S. Y. Noh, Y. Jing, S. Jin, P. K. L. Yu and D. Wang, *Energy Environ. Sci.*, 2012, **5**, 7872–7877.
26 N. C. Strandwitz, D. J. Comstock, R. L. Grimm, A. C. Nichols-Nielander, J. Elam and N. S. Lewis, *J. Phys. Chem. C*, 2013, **117**, 4931–4936.
27 A. Kargar, K. Sun, Y. Jing, C. Choi, H. Jeong, G. Y. Jung, S. Jin and D. Wang, *ACS Nano*, 2013, **7**, 9407–9415.
28 L. Trotochaud, J. K. Ranney, K. N. Williams and S. W. Boettcher, *J. Am. Chem. Soc.*, 2012, **134**, 17253–17261.
29 T. K. Townsend, N. D. Browning and F. E. Osterloh, *Energy Environ. Sci.*, 2012, **5**, 9543–9550.
30 C. C. L. McCrory, S. Jung, J. C. Peters and T. F. Jaramillo, *J. Am. Chem. Soc.*, 2013, **135**, 16977–16987.
31 M. Gong, W. Zhou, M.-C. Tsai, J. Zhou, M. Guan, M.-C. Lin, B. Zhang, Y. Hu, D.-Y. Wang, J. Yang, S. J. Pennycook, B.-J. Hwang and H. Dai, *Nat. Commun.*, 2014, **5**, 4695.
32 C.-Y. Lin, Y.-H. Lai, D. Mersch and E. Reisner, *Chem. Sci.*, 2012, **3**, 3482–3487.
33 F. P. Koffyberg and F. A. Benko, *J. Electrochem. Soc.*, 1981, **128**, 2476–2479.
34 H. Kato, K. Asakura and A. Kudo, *J. Am. Chem. Soc.*, 2003, **125**, 3082–3089.
35 F. E. Osterloh, *Chem. Mater.*, 2007, **20**, 35–54.
36 F. E. Osterloh, *Chem. Soc. Rev.*, 2013, **42**, 2294–2320.
37 L. Vayssieres, N. Beermann, S.-E. Lindquist and A. Hagfeldt, *Chem. Mater.*, 2000, **13**, 233–235.
38 A. Kargar, S. J. Kim, P. Allameh, C. Choi, N. Park, H. Jeong, Y. Pak, G. Y. Jung, X. Pan, D. Wang and S. Jin, *Adv. Funct. Mater.*, 2015, under minor revision.
39 J. R. McKone, E. L. Warren, M. J. Bierman, S. W. Boettcher, B. S. Brunschwig, N. S. Lewis and H. B. Gray, *Energy Environ. Sci.*, 2011, **4**, 3573–3583.
40 K. Sun, K. Madsen, P. Andersen, W. Bao, Z. Sun and D. Wang, *Nanotechnology*, 2012, **23**, 194013.